

Final Draft

of the original manuscript:

Winzer, N.; Atrens, A.; Dietzel, W.; Song, G.; Kainer, K.U.:

**Comparison of the Linearly Increasing Stress Test and the
Constant Extension Rate Test in the Evaluation of Transgranular
Stress Corrosion Cracking of Magnesium**

In: Materials Science and Engineering A (2007) Elsevier

DOI: 10.1016/j.msea.2007.03.021

Comparison of the Linearly Increasing Stress Test and the Constant Extension Rate Test in the Evaluation of Transgranular Stress Corrosion Cracking of Magnesium

N. Winzer^{a,b}, A. Atrens^{a,b}, W. Dietzel^b, G. Song^a, K.U. Kainer^b

^a Materials Engineering, The University of Queensland
Brisbane Australia 4072
a.atrens@minmet.uq.edu.au

^b Institute for Materials Research, GKSS-Forschungszentrum Geesthacht GmbH,
D-21502 Geesthacht Germany

Abstract

Transgranular stress corrosion cracking (TGSCC) of the Mg alloy AZ91 in distilled water and 5 g/L NaCl solution has been evaluated using the Linearly Increasing Stress Test (LIST) and the Constant Extension Rate Test (CERT). The differences between these techniques, with respect to fractography and the measurement of SCC parameters, are discussed. The LIST and CERT techniques are both useful in identifying the occurrence of SCC and, when coupled with a technique for characterizing crack extension, measuring the threshold stress and crack velocity. During a LIST, fast fracture ensues a relatively short time after the threshold stress is attained, whereas during CERT crack growth over a much longer time period is facilitated by a reduction in stress. Consequently, the LIST is typically 30 – 50 % shorter in duration, whereas the CERT produces a larger SCC fracture surface.

Keywords: Stress Corrosion Cracking; Magnesium; Linearly Increasing Stress Test; Constant Extension Rate Test; Fractography; Hydrogen

1 Introduction

Our recent critical review [1] described two commonly used methods for characterizing SCC: the Linearly Increasing Stress Test (LIST) and the Constant Extension Rate Test (CERT). In the LIST and CERT the nominal load and extension is increased until specimen fracture, respectively. Neither method accurately simulates operating conditions; however, they allow more rapid characterization of SCC susceptibility compared to constant load tests and permit direct measurement of critical parameters such as the threshold stress (σ_{SCC}) and crack velocity (V_C) when coupled with equipment to measure crack extension.

SCC of Mg alloys is inherently transgranular and somehow involves cathodically produced H entering the metal substrate. The specific nature of the mechanism for TGSCC in Mg alloys is still highly equivocal. The most commonly proposed mechanism is Delayed Hydride Cracking, which involves repeated stages of stress-assisted diffusion of H ahead of the crack tip leading to hydride formation and fracture [2, 3, 4, 5]. H Enhanced Localized Plasticity (HELP) resulting from adsorption of H atoms at the crack tip has also been suggested, particularly for higher crack velocities [6]. Considering the wide range of crack velocities reported by previous workers it is conceivable that both mechanisms are possible and that the predominant mechanism is related to crack velocity.

The competition between DHC and HELP may be defined by the propensity for solute H to diffuse ahead of the crack tip, which is dependent on: (i) the tendency for H to enter the substrate and cause crack initiation; and (ii) the stress distribution at the crack tip. H ingress may occur as a result of mechanically or chemically induced film rupture. Thus, mechanical conditions applied by the SCC test apparatus may influence the balance between the two competing mechanisms, such that the choice of test method may have an effect on the SCC parameters being measured.

2 Experimental Method

The LIST apparatus [8] is illustrated in Figure 1. The specimen is attached to one end of a lever arm. To the opposite end of the arm a known mass is attached such that the tensile load applied to the specimen increases linearly as the distance between the fulcrum and the mass is increased by means of a screw thread and synchronous motor. The CERT apparatus used in this study (Figure 2, [7]) maintained a constant strain rate by means of an open-loop control system; the average strain was measured by two high-resolution LVDTs in parallel with the specimen and a geared synchronous motor increased the strain accordingly.

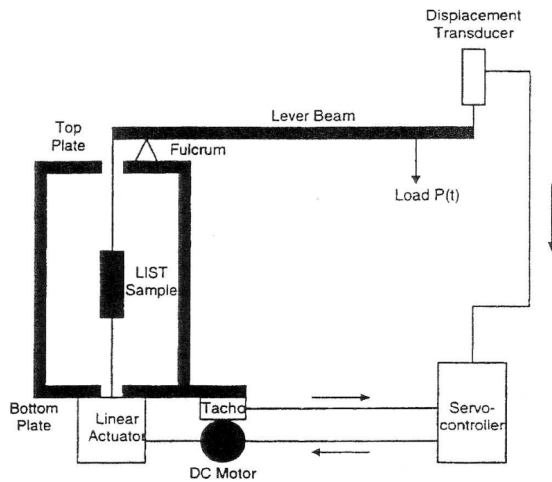


Figure 1 - Schematic illustration of LIST apparatus.

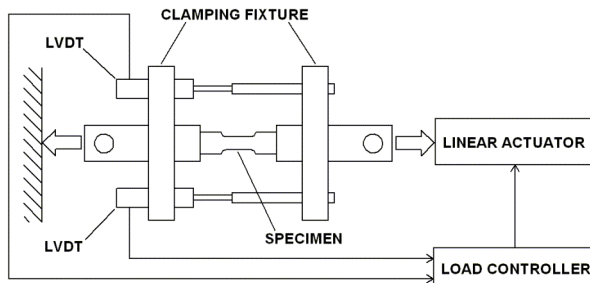


Figure 2 - Schematic illustration of CERT apparatus.

All tests were performed using high purity AZ91 alloy (>90.11wt%Mg, 8.99wt%Al, 0.78wt%Zn, 0.21wt%Mn). Cylindrical tensile specimens with 5 mm diameter waisted gauge were machined from as-cast ingots according to the dimensions shown in Figure 3. The gauge surface was polished with 600 grit emery paper and the specimens were degreased in ethanol before use. The test environments were 5g/L NaCl solution, double-distilled water and laboratory air. All solutions were made from reagent grade chemicals and double-distilled water. All tests were conducted at open-circuit conditions. Fracture surfaces were cleaned in chromic acid before SEM examination.

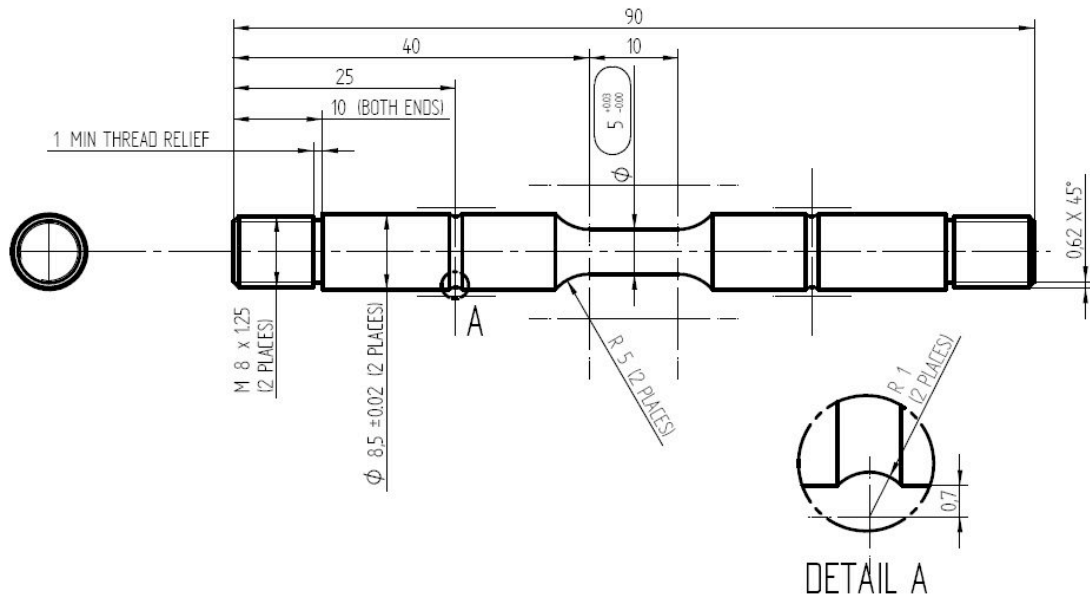


Figure 3 – Technical schematic of specimens.

Back-scatter electron detection of polished sectioned tensile specimens showed that the grain size was typically 50 μm . Energy dispersive X-ray spectroscopy (EDS) of polished sectioned tensile specimens revealed four distinct phases: the bulk matrix (approximately 95wt%Mg, 4wt%Al and 0.5wt%Zn); an extensive interdendritic phase (approximately 58wt%Mg, 37wt%Al, 5wt%Zn); fine plate-like crystals within the interdendritic phase (approximately 28wt%Mg, 47wt%Al, 23wt%Mn, 1wt%Zn); and small intragranular precipitates (approximately 2.5wt%Mg, 43wt%Al, 54wt%Mn, 0.5wt%Zn). The phases are shown in Figure 4.

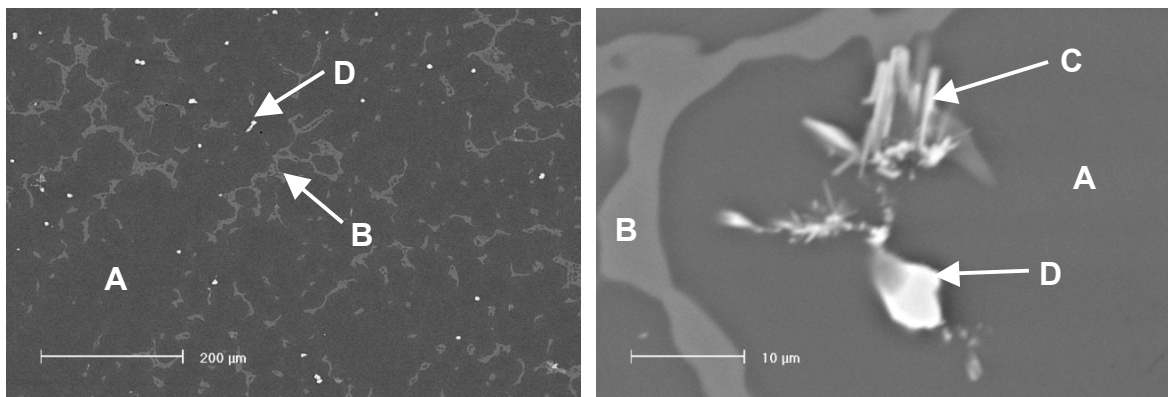


Figure 4 – Back-scatter electron images of polished sectioned tensile specimens showing (A) bulk matrix, (B) interdendritic phase, (C) plate-like crystals and (D) intragranular precipitates.

SCC susceptibility was characterised according to the threshold stress, which was determined using the DC potential drop (DCPD) method as per Atrens et al [8, 9, 10, 11, 12]. The DCPD method involves applying a low constant current to the specimen and measuring the change in specimen resistance as the cross-section is reduced, primarily by crack propagation, according to the relationship $\Delta R = \rho l / \Delta A$, where ΔA is the change in cross-sectional area, ρ is the resistivity and l is the length of the specimen. LIST tests were performed with a basic DCPD system as described in Winzer et al [13]. The resistance of the specimen was measured with insufficient resolution to accurately determine the SCC parameters. CERT tests were performed using a more advanced DCPD system as described in Dietzel et al. [14]. A pulsed and reversing current was applied to the specimen to minimise thermoelectric offset voltages due to coupling of dissimilar metals in a variable-temperature environment. Variations in the resistivity of the

specimen due to temperature were accounted for by using a reference specimen. These features enabled the SCC parameters to be characterised with considerably higher resolution and greater repeatability.

3 Results

3.1 Determination of Threshold Stress

Figures 5, 6, 7 and 8 show the stress-strain behaviour and DCPD measurements for CERTs at four different strain rates in distilled water and in air. For the specimens tested in distilled water there was a considerable reduction in the UTS relative to air, with the UTS clearly decreasing with decreasing strain rate, as shown in Figures 5 and 6. The threshold stress was interpreted as being the point where the DCPD curve became significantly non-linear, as shown in Figure 7. The threshold stress in distilled water at 3×10^{-8} , 10^{-7} , 3×10^{-7} and 5×10^{-7} s^{-1} was between 55 MPa and 75 MPa. The resolution of the DCPD system and the small change in potential during early crack propagation limited the precision of the threshold stress measurement to ± 5 MPa. The threshold stress values measured in 5g/L NaCl solution were somewhat lower than for distilled water (55 MPa at 1×10^{-7} s^{-1} and 65 MPa at 3×10^{-7} s^{-1} and 5×10^{-7} s^{-1}). In both environments there was an apparent tendency for a lower threshold stress at lower strain rates.

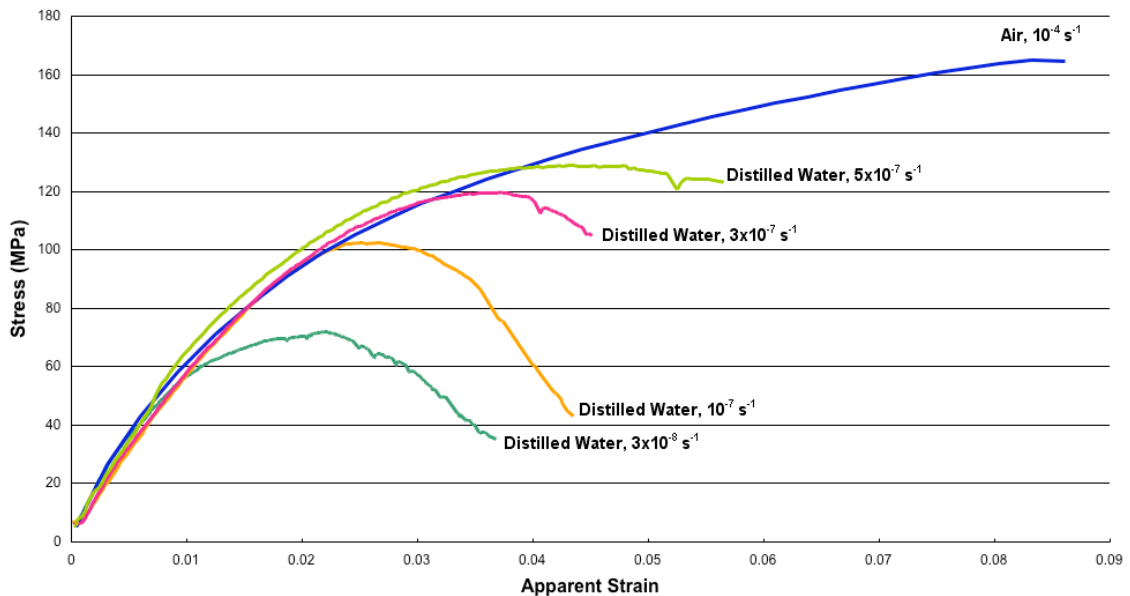


Figure 5 - Stress-strain curves for AZ91 in distilled water and air.

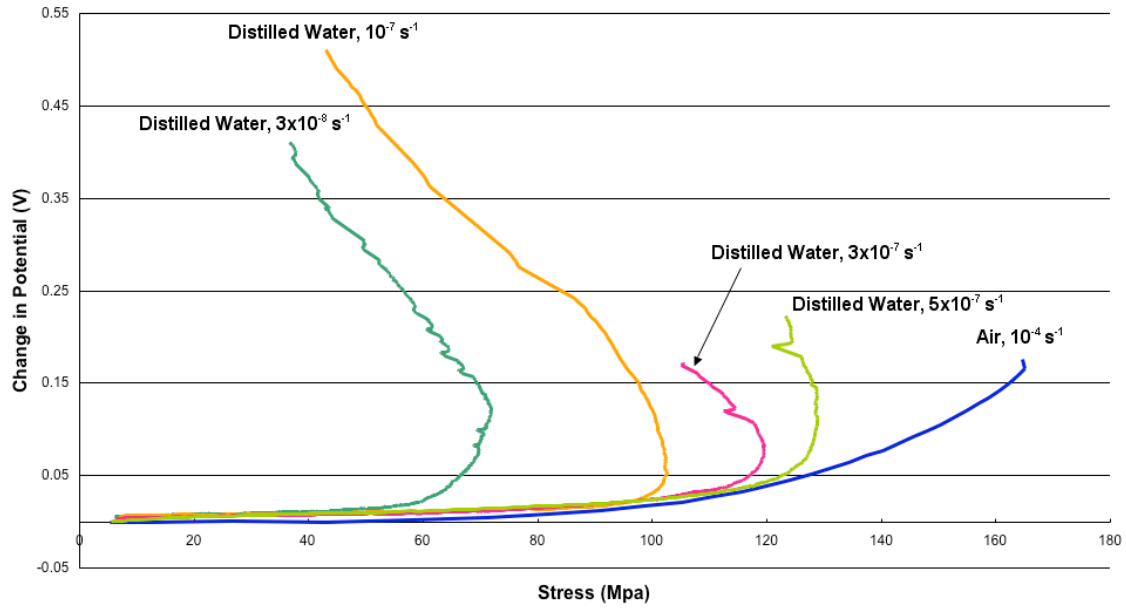


Figure 6 - DCPD results for AZ91 in distilled water and air.

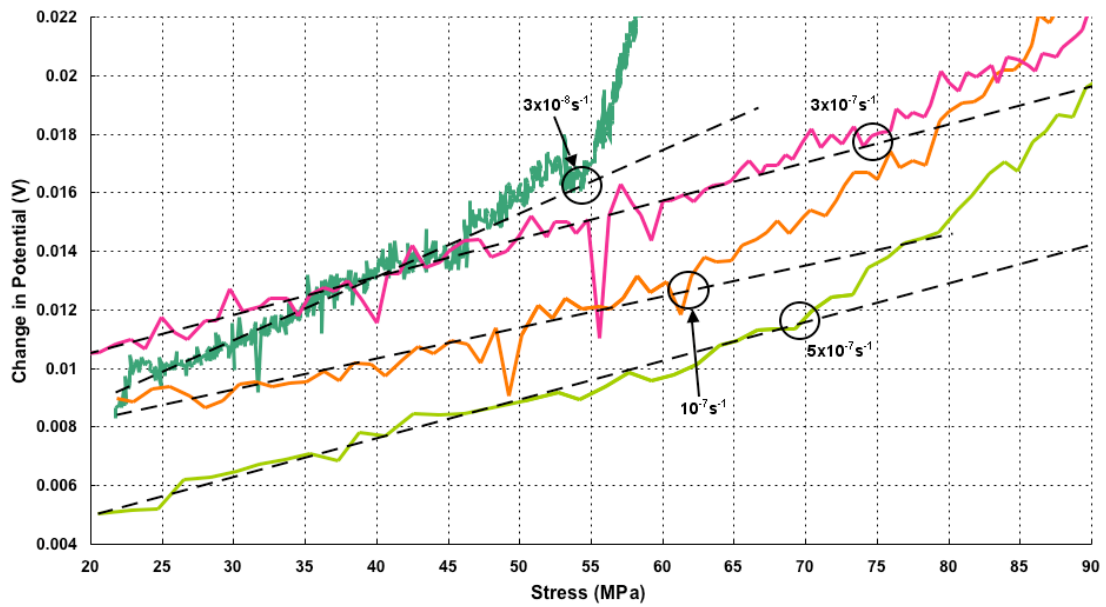


Figure 7 - DCPD results for AZ91 in distilled water and air showing threshold stresses.

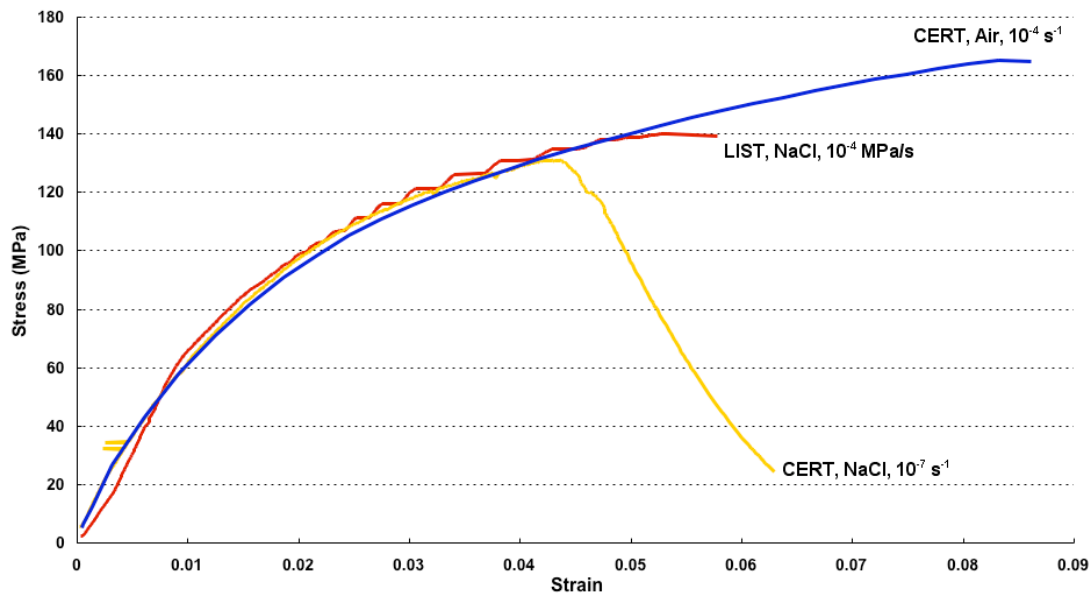


Figure 8 - Comparison between stress-strain results for LIST and CERT.

The correlation between the threshold stress and the deviation of the DCPD curve from its initial linearity was confirmed by immersing a specimen in distilled water at a constant stress of 60 MPa for ~200 hrs. The specimen was subsequently immersed in dye penetrant and fractured abruptly in air. Examination of the fracture surface revealed a macroscopically flat die-marked region corresponding to SCC, as shown in Figure 9 (see below for description of the SCC fracture surface).



Figure 9 – Stereomicroscope and SEM images of fracture surface for specimen immersed in distilled water at 60 MPa for ~200 hrs.

Figure 8 shows a comparison between a LIST and a CERT at 7.3×10^{-4} MPa/s and 10^{-7} s⁻¹, respectively, under identical environmental conditions. These loading rates are equivalent for purely elastic behaviour. A LIST was typically complete soon after crack initiation; fast fracture occurred when the crack reached a critical size for the applied load. In contrast stress corrosion cracks during a CERT propagated for a long period of time. A CERT was typically 2 to 3 times longer in duration and was sometimes manually stopped after a significant reduction in nominal stress had occurred. Figure 8 also shows that considerable crack propagation occurs even after the nominal stress is reduced to a value below the threshold stress; however, this effect is primarily due to the reduction in cross sectional area of the specimen by crack propagation.

3.2 Fractography

The fracture surfaces for CERT specimens in distilled water were partly comprised of macroscopically flat regions penetrating up to $\sim 1000\ \mu\text{m}$ from the gauge surface (Figure 10), with the depth of penetration increasing with decreasing strain rate. These regions were interpreted as being due to SCC. The SCC regions were generally characterised by: (i) coarse parallel markings typically $\sim 5\ \mu\text{m}$ apart; (ii) jogging at the edges of each step; and (iii) secondary cracking. The parallel markings are unidirectional within a discrete area; however, their direction may differ from other regions with changes in direction occurring at intervals corresponding to the grain size. Closer examination revealed that some parallel markings constituted cleavage-like facets with adjoining steps (Figure 10, Detail C), whereas others constituted pyramidal crevices or “flutes” with reduced jogging (Figure 11). Examination under high magnification revealed that the regions between consecutive parallel markings were comprised of fine parallel markings (typically $<0.5\ \mu\text{m}$ apart) or micro-dimples (Figure 11, Detail B and Detail C); however, at this magnification it was difficult to differentiate between the two. The perpendicular markings are clearly influenced by crystallography, as evidenced by perpendicular changes in direction (Figure 12). Cleavage of the β -precipitates in line with the SCC crack plane and micro-galvanic corrosion at the α - β interface are also evident (Figures 12 and 13). The β -precipitates also appear to influence the orientation of the coarse parallel markings (Figure 13). In this case the fracture of the β -particle appears to have initiated fracture in the α -phase on the left hand side of the β -particle.

The remaining fracture surface had identical features as samples tested in air and were interpreted as being due to final overload fracture. These regions were characterised by broken, jagged facets randomly interspersed with cleavage-like regions typically $<20\ \mu\text{m}$ across (Figure 14).

Early crack propagation under CERT conditions was investigated by immersing specimens in distilled water at $5 \times 10^{-7}\ \text{s}^{-1}$ and interrupting the test at various stresses above the threshold stress. The specimens were subsequently fractured abruptly in air. The resulting fracture surfaces were partly comprised of macroscopically smooth regions at the gauge surface (Figure 15). The depth of penetration of these regions was $<100\ \mu\text{m}$. Examination under high magnification revealed that these regions were comprised of fine parallel markings and micro-dimples similar to those shown in Figure 11, Detail C and Figure 12.

Figure 16 shows the fracture surface for a specimen tested in 5 g/L NaCl at $10^{-7}\ \text{s}^{-1}$ under CERT conditions. There was extensive pitting with some pits penetrating $\sim 400\ \mu\text{m}$ from the surface. The fracture surface associated with SCC corresponded to macroscopically flat fracture surface regions containing coarse parallel markings, similar to those observed for distilled water. Again, these regions comprised a high proportion of the total fracture surface area. Furthermore, these regions showed much less pitting than on the specimen surface, and the pits were much more shallow than on the specimen surface. The remaining fracture surface was comprised of the broken, jagged features shown in Figure 14 and typical of final overload fracture.

Fracture surfaces for tests in 5 g/L NaCl solution under LIST conditions primarily consisted of the broken, jagged features associated with overload fracture, with highly localized areas at the gauge surface containing coarse parallel markings, as shown in Figure 17. The regions containing parallel markings were generally $<100\ \mu\text{m}$ across. The markings were generally similar to those associated with SCC of CERT specimens in distilled water.

4 Discussion

4.1 Limits of SCC Susceptibility

Figures 6 and 7 show that for AZ91 tested in distilled water at $3 \times 10^{-8}\ \text{s}^{-1}$ to $5 \times 10^{-7}\ \text{s}^{-1}$ there was a reduction in UTS relative to air that is indicative of SCC. Ebtehaj et al [15] and Wearmouth et al [16] proposed that for Mg-Al alloys, in solutions containing approximately equal concentrations of chloride and chromate ions, maximum SCC susceptibility occurred at a discrete range of intermediate strain rates at $\sim 10^{-5}\ \text{s}^{-1}$; at low strain rates repassivation retards H-ingress at mechanical film rupture sites whereas at

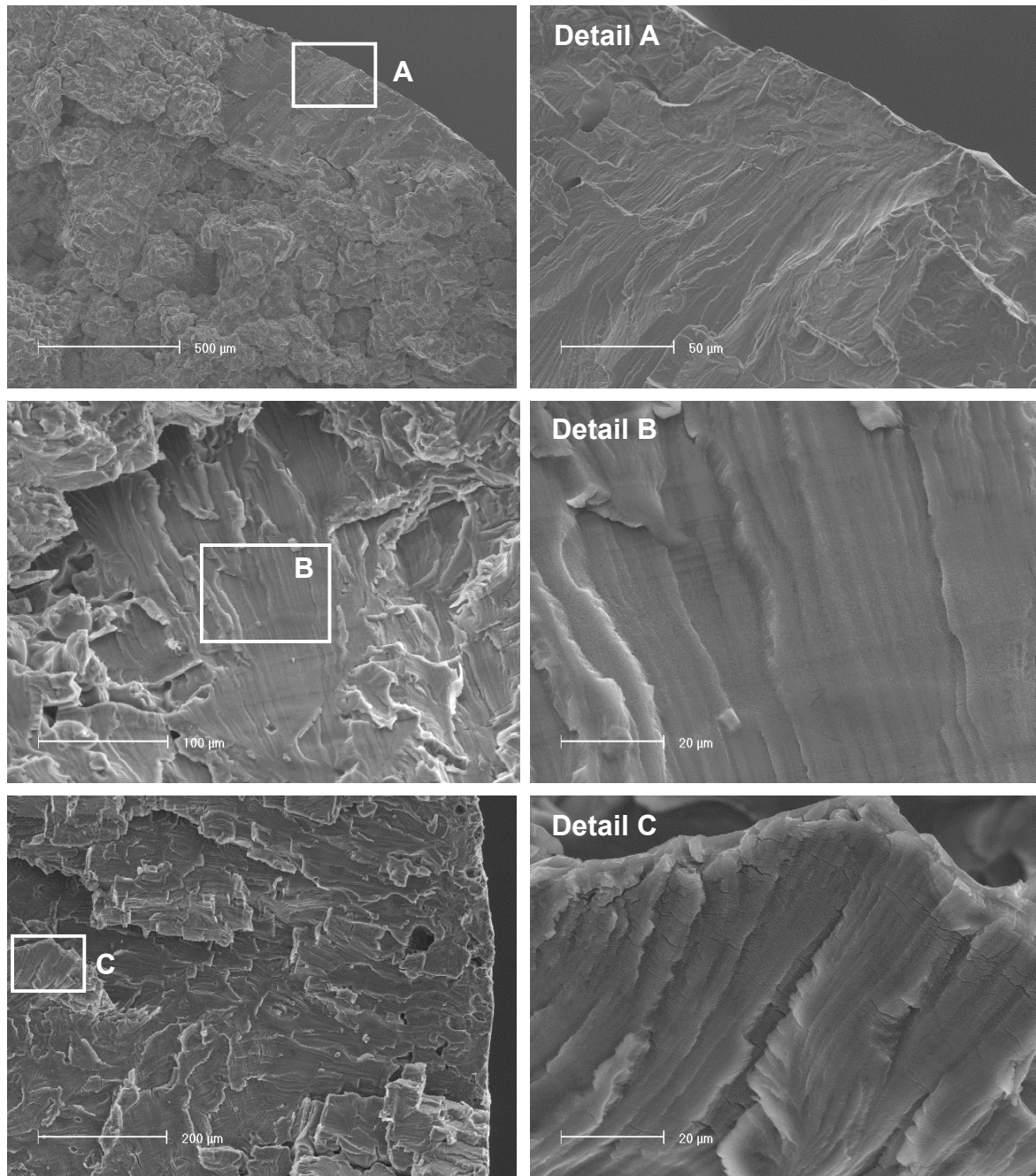


Figure 10 - SEM micrographs of specimen fractured in distilled water at $3 \times 10^{-8} \text{ s}^{-1}$ showing appearance of macroscopically flat regions at gauge surface (Detail A), parallel markings (Detail B) and joggling (Detail C).

high strain rates ductile tearing predominates. In the present study, the UTS and threshold stress decreased with decreasing strain rate at strain rates much lower than those intermediate strain rates below which an increase in “ductility” was observed by Ebtehaj et al [15] and Wearmouth et al [16]. This suggests that there was no effective repassivation in the present study at the lower strain rates, and consequently no barrier to hydrogen ingress. This implies that the maximum in SCC susceptibility for Mg alloys in solutions containing chloride and chromate ions is a particular feature of these solutions and is not an inherent aspect of the Mg SCC mechanism.

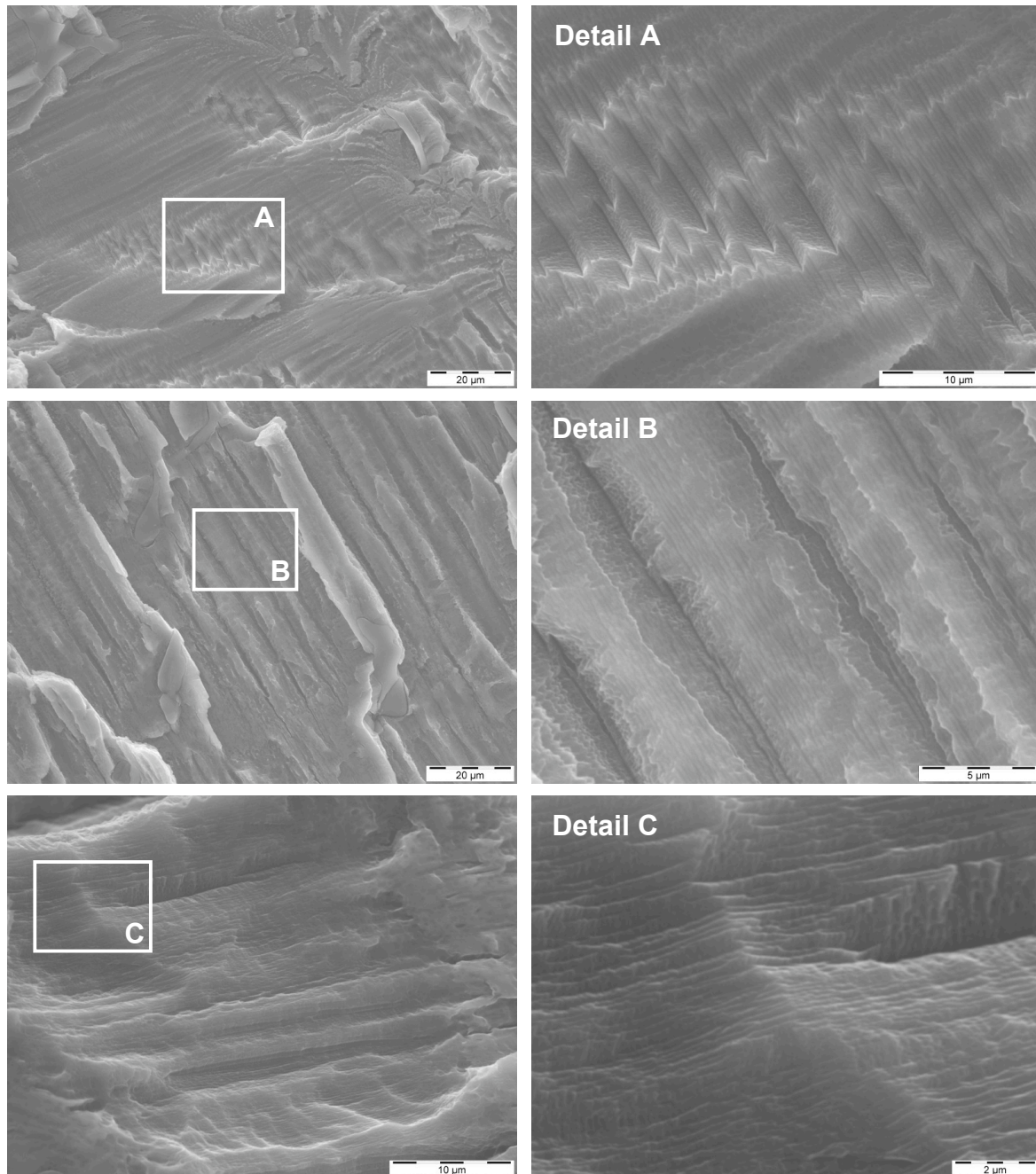


Figure 11 - SEM micrographs of specimen fractured in distilled water at 10^{-7} s^{-1} showing appearance of pyramidal crevices (Detail A), curved facets or flutes (Detail B) and fine parallel markings or micro-dimples (Detail C).

4.2 *Distilled Water vs NaCl*

Specimens fractured in distilled water had lower UTS's than those in 5g/L NaCl. No pitting was observed after exposure to distilled water whereas exposure to 5 g/L NaCl resulted in severe pitting. This suggests that H ingress in distilled water is dependent on mechanical film rupture. For specimens exposed to the 5g/L NaCl solution, H ingress may have been partly inhibited by excessive dissolution as proposed by Ebtehaj et al [15] and Makar et al [17]. In other words, the rate of localized corrosion was greater than the rate of hydrogen diffusion.

4.3 Fractography

The fracture surfaces observed for tests in distilled water and 5 g/L NaCl solution were consistent with those observed by Stampella et al [18] for pure Mg anodically polarized in Na₂SO₄ solution, Meletis and Hochman [2] for pure Mg in NaCl-K₂CrO₄ solution and Chakrapani and Pugh [19] and Wearmouth et al [16] for Mg-7.5Al in NaCl-K₂CrO₄ solutions. These fracture surfaces are characterised by coarse parallel markings, secondary cracking and jogging. That the regions containing the parallel markings were located invariably at or close to gauge surfaces suggests that they correspond to crack initiation sites. Meletis and Hochman proposed that the parallel facets and joining perpendicular steps were primarily due to cleavage on {2 $\bar{2}$ 03} planes parallel to the direction of crack propagation. Since there are six {2 $\bar{2}$ 03} planes in the HCP crystal lattice, cleavage results in crystallographic 3-dimensional fracture surfaces. This is evidenced by the change in direction of parallel facets as they cross grain boundaries and jog formation, which results from overlapping cracks. Such crystallography may be related to the formation and fracture of brittle hydride platelets on preferential planes, which is a known mechanism for H-induced cracking in other metals (particularly Zr, Nb, V, Ta and Ti and their alloys) [20, 21, 22, 23]. The fracture surfaces observed in the present study may be correlated with those for DHC in Zr [24, 25]; however, it should be noted that the distances between consecutive parallel markings is considerably less than for Zr fracture.

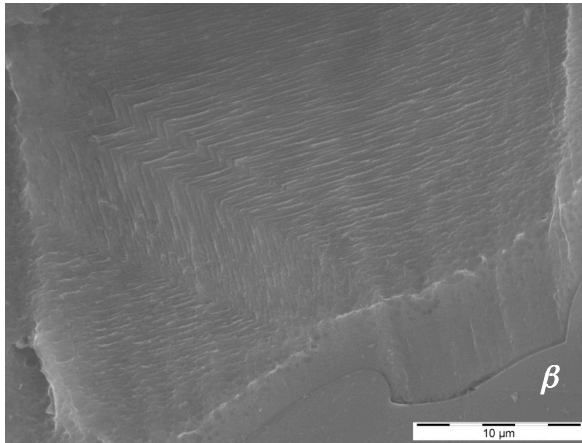


Figure 12 – Fine parallel markings, cleavage through β and micro-galvanic corrosion at α - β interface

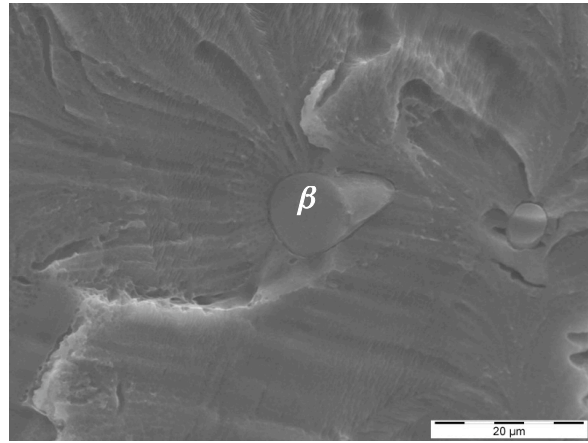


Figure 13 – The influence of β precipitates on the direction of coarse parallel markings.

It is unclear whether the micro-dimples within steps are artifacts of a ductile tearing process (possibly associated with crack arrest at the hydride platelet boundary), a secondary process associated with plastic accommodation of the hydride or a separate HE mechanism involving microvoid coalescence. Such a mechanism was proposed by Lynch and Trevena [6] to explain crystallographic, fluted fracture surfaces for SCC in pure Mg exposed to NaCl-K₂CrO₄ solution. The appearance of pyramidal crevices or flutes containing micro-dimples (Figure 11, Detail A and Detail B) is further evidence of the prevalence of this mechanism. Lynch and Trevena proposed that microvoid coalescence resulted from emission of dislocations from the crack leading due to adsorption of H atoms. Due to the dependence on adsorption rather than diffusion, the mechanism could sustain much higher crack velocities than a mechanism involving diffusion of H ahead of the crack tip (such as DHC). Since the crack front is highly irregular, it is conceivable that velocities at different points of the crack front may differ considerably. Thus, if the local predominant mechanism is dependent on the crack velocity, then there may be more than one mechanism active at a particular time during crack propagation.

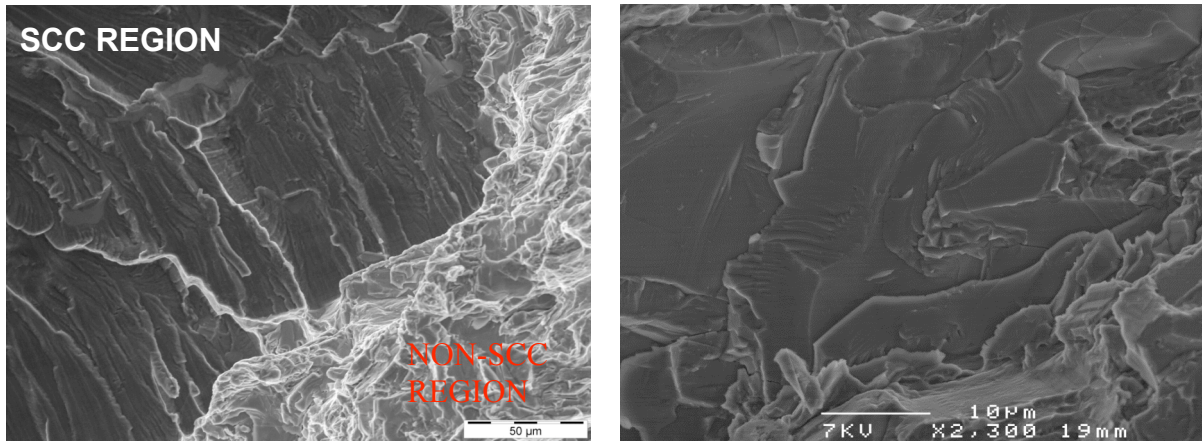


Figure 14 - SEM micrographs of typical overload fracture surfaces.

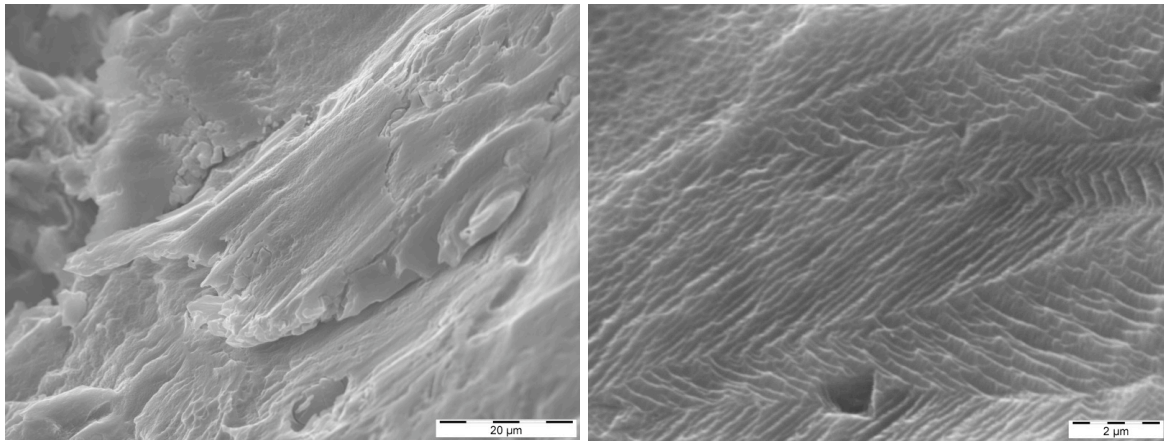


Figure 15 – SCC fracture surface for CERT specimens interrupted at stresses above σ_Y .

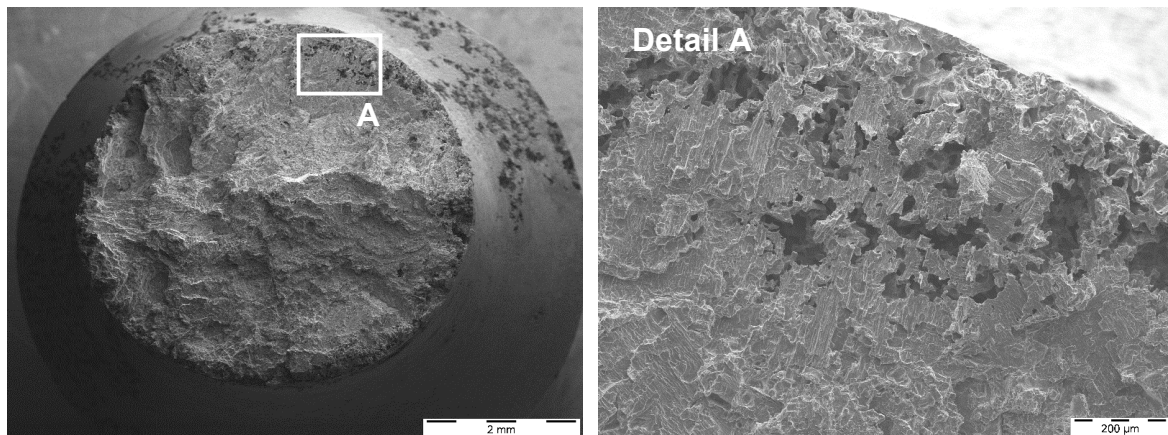


Figure 16 - SEM micrographs of specimens fractured in 5g/L NaCl at 10^{-7} s^{-1} .

4.4 Mechanistic Considerations

TGSCC of Mg is associated with conditions causing electrochemical breakdown or mechanical rupture of protective films at the crack surface, which allow H to enter the metal substrate [1]. Furthermore, it is

likely that the mechanism for steady-state crack propagation in TGSCC of Mg alloys involves stress directed diffusion of H ahead of the crack tip [1]. Thus, any mechanistic differences in TGSCC of Mg alloys under LIST and CERT conditions should be rationalized in terms of differences in the crack tip stress fields over time or the processes involved in breakdown/rupture of protective films at the crack surface.

A possible mechanistic difference may be derived from the assumption that the mechanism for crack propagation involves repetitive formation and fracture of a brittle zone by stress-assisted diffusion of H ahead of the crack tip (as per DHC). Under LIST conditions the load is relatively constant for consecutive stages of crack advance. Consequently, the stress intensity at the crack tip, and the driving force for H diffusion, would also be relatively constant (although the stress intensity at the crack tip may be reduced somewhat by blunting, a possible cause of crack arrest). In contrast, under CERT conditions there is a reduction in load, as shown in Figures 6 and 7, with crack propagation. Thus, there is a potential reduction in driving force for H diffusion and an increase in the time available for repassivation at the crack surface.

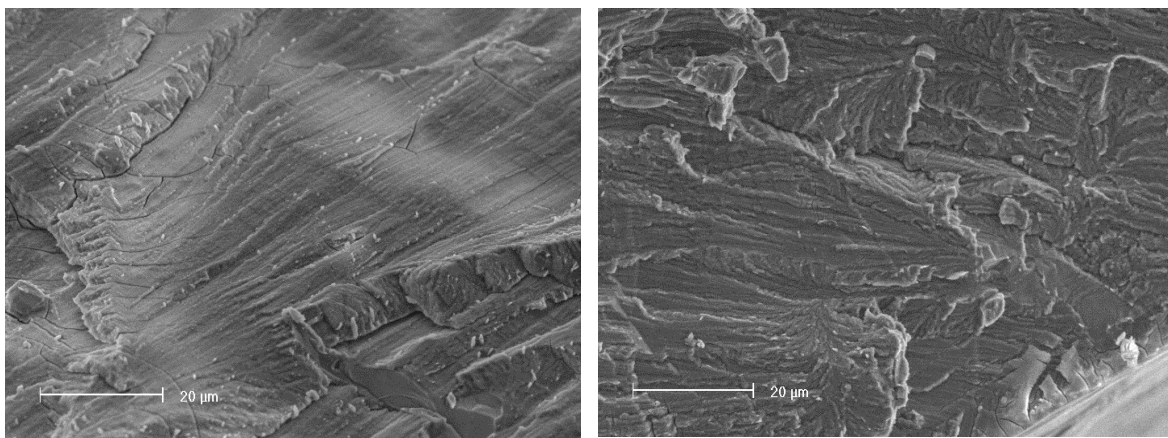


Figure 17 - SEM micrographs of AZ91 in distilled water at 7.3×10^{-4} MPa/s.

That LISTs in SCC-causing environments result in small, localised regions of parallel markings suggests that when the applied stress reaches σ_{SCC} , H-embrittlement causes the crack to propagate until some critical crack length is reached a short distance from the surface. Here the crack propagation mechanism is overwhelmed by some non-H-assisted process such as cleavage or microvoid coalescence. In contrast, the CERTs result in considerably larger regions of parallel markings. This may be attributed to a tendency for stress relaxation coupled with crack tip opening displacement; as the crack propagates some distance stress may be reduced below the threshold or the local stress at the crack tip may be reduced such that the HE processes are retarded. These tendencies underpin the principal differences between the two methods; CERTs lend themselves to easier fractography and fracture surface analysis whereas LISTs are more rapid owing to their tendency for fast fracture once the critical crack length is reached.

That the SCC fracture surfaces resulting from the interrupted CERTs (Figure 15) are macroscopically different to the those corresponding to later-stage crack propagation under CERT conditions is also indicative of a load-dependence of the predominant mechanism. This may be due to relatively low stress intensity at the crack tip during early crack propagation.

5 Conclusions

LIST and CERT have been used in an ongoing program to develop a mechanistic understanding of the environmental and mechanical factors influencing SCC of Mg alloys. From these results it is apparent that the LIST provides more rapid determination of the threshold stress, whereas the CERT provides

larger fracture surface area for analysis and increased crack propagation time for determining the overall steady-state crack velocity. It follows that the LIST method may be more suitable for investigating SCC in aggressive environments where pitting may be a consideration, although it should be noted that in very aggressive environments localized dissolution of the metal may outrun the SCC mechanism altogether. The increased crack propagation time under CERT conditions may be particularly important in determining the underlying mechanism for SCC in Mg alloys, since the predominant mechanism is somehow related to the crack velocity. However, it must be remembered that stress corrosion crack growth occurs under conditions of decreasing load, and the fractography towards the end of a CERT may not be typical of that in the earlier stages of stress corrosion cracking. SCC testing in distilled water and 5 g/L NaCl under CERT conditions showed that maximum susceptibility occurred in distilled water at the slowest strain rate. It should be noted that the mechanism for TGSCC is dependent on the stress distribution near the crack tip and the propensity for film rupture and repair at crack surface. Consequently there are potential mechanistic differences for TGSCC of Mg alloys under LIST and CERT conditions.

6 Acknowledgements

The authors wish to thank the GM Technical Centre at Warren MI, the Australian Research Council (ARC) and the Australian Research Network for Advanced Materials (ARNAM). N. Winzer and A. Atrens wish to thank GKSS Forschungszentrum Geesthacht for allowing them to visit between 2005 and 2007. V. Heitmann and U. Burmeister, both of GKSS Forschungszentrum Geesthacht are thanked for their assistance with experiments and fractography.

7 References

- [1] N. Winzer, A. Atrens, G. Song, E. Ghali, W. Dietzel, K.U. Kainer, N. Hort and C. Blawert, *Adv. Eng. Mater.*, 2005, 7, No. 8, pp. 659-693
- [2] E.I. Meletis, R.F. Hochman, *Corrosion*, 1984, 40, pp. 39-45
- [3] D.G. Chakrapani, E.N. Pugh, *Metall. Trans. A*, 1976, 7A, pp. 173-178
- [4] G.L. Makar, J. Kruger, K. Sieradzki, *Corros. Sci.*, 1993, 34, No. 8, pp. 1311-1342
- [5] N. Winzer, A. Atrens, W. Dietzel, G. Song, K.U. Kainer, *Mater. Sci. Eng. A* (2007), doi:10.1016/j.msea.2007.03.020.
- [6] S.P. Lynch, P. Trevena, *Corrosion*, 1988, 44, pp. 113-124
- [7] W. Dietzel, K.H. Schwalbe, in: *ASTM STP 1210: Slow Strain Rate Testing for the Evaluation of Environmentally Induced Cracking: Research and Engineering Applications*; R. D. Kane (Ed.), ASTM, 1993, pp. 134-148.
- [8] A. Atrens, C.C. Brosnan, S. Ramamurthy, A. Oehlert, I.O. Smith, *Meas. Sci. Technol.*, 1993, 4, pp. 1281-1292
- [9] A. Oehlert, A. Atrens, *J Mater. Sci.*, 1998, 33, pp. 775-781
- [10] A. Oehlert, A. Atrens, *J Mater. Sci.*, 1997, 32, pp. 6519-6523
- [11] A. Oehlert, A. Atrens, *Corros. Sci.*, 1996, 38, pp. 1159-1170
- [12] A. Oehlert, A. Atrens, *Acta Metall. Mater.*, 1994, 42, pp. 1493-1508
- [13] N. Winzer, G. Song, A. Atrens, W. Dietzel and C. Blawert, *Corrosion and Prevention 2005*, ACA, 37
- [14] W. Dietzel, K.-H. Schwalbe, *Z. Materialprüfung/Materials testing*, 1986, 28, No 11, pp. 368-372
- [15] K. Ebtehaj, D. Hardie, R.N. Parkins, *Corros. Sci.*, 1993, 28, pp. 811-829
- [16] W.R. Wearmouth, G.P. Dean, R.N. Parkins, *Corrosion*, 1979, 29, No 6, pp. 251-258
- [17] G.L. Makar, J. Kruger, K. Sieradzki, *Corros. Sci.*, 1993, 34, pp. 1311-1342
- [18] R.S. Stampella, R.P.M. Proctor, V. Ashworth, *Corros. Sci.*, 1984, 24, No 4, pp. 325-341
- [19] D.G. Chakrapani, E.N. Pugh, *Corrosion*, 1975, 31, pp. 247-252

-
- [20] S.P. Lynch, in: N.R. Moody, A.W. Thompson, R.E. Ricker, G.W. Was, R.H. Jones (Eds.), Hydrogen Effects on Material Behaviour and Corrosion Deformation Interactions, TMS, 2003, pp. 449-466
- [21] C.E. Coleman, in: I. Milne, R.O. Ritchie, B. Karihaloo (Eds.), Comprehensive Structural Integrity, Elsevier Ltd, Vol. 6, pp. 103-161
- [22] H.K. Birnbaum, in: N.R. Moody, A.W. Thompson (Eds.), Hydrogen Effects on Material Behaviour, TMS, 1990, pp. 639-660
- [23] B. Cox, J Nucl. Mater., 1990, 170, pp. 1-23
- [24] B. Cox, Proceedings of the Metallography and Corrosion Symposium, NACE, 1983, pp. 153-174
- [25] L.A. Simpson, in: K.J. Miller, R.A. Smith (Eds.), Mechanical Behaviour of Materials, ICM, 1979, Vol 2, pp. 445-455